

Modeling High-Power Density Thermoelectric Assemblies Which Use Thermal Isolation

D.T. Crane
 BSST, LLC
 5462 Irwindale Avenue, Irwindale, CA 91706-2058 USA
 1-626-815-7400 x 1048 1-626-815-7438 (fax)
 dcrane@bsst.com

Abstract

A numerical model comprised of simultaneously solved, non-linear, energy balance equations has been created to simulate high-power density thermoelectric (TE) assemblies, which utilize thermal isolation in heating and cooling applications. In the devices modeled, TE elements are incorporated into liquid-liquid heat exchangers that eliminate many of the loss mechanisms for a conventional TE assembly, including the ceramic electrical isolation layer. The model predicts data from experiments of advanced thermodynamic cycles in various configurations to less than 7% error for coefficient of performance (COP), input power, and mass flow rates over a broad range of temperatures and currents.

The ability to accurately and precisely model such devices further confirms the concept of improving device COP through the use of thermal isolation, since the devices being modeled show about a factor of two improvement in COP over a conventional TE configuration for the same conditions. Such a model also allows the device to be extensively studied without additional experimentation. Using advanced multi-parameter optimization techniques, the devices can be optimized for a set of temperature and flow conditions.

Introduction

In 2002, Bell [1] first introduced and Diller and Chang [2] experimentally proved the concept of thermal isolation in the direction of flow as a thermodynamic cycle that can significantly improve the coefficient of performance of a thermoelectric or any other electrical to thermal direct energy conversion device. To further explore the benefits of thermal isolation, a numerical model has been created in a MATLAB environment. Building on previous work of TE numerical simulation [3, 4], this steady-state model is comprised of simultaneously solved, non-linear, energy balance equations. These energy balance equations simulate high-power density TE assemblies, see Figure 1, which utilize thermal isolation in heating and cooling applications.

The high-power density heat exchanger, see Figure 1, is made up of a series of individual copper heat exchangers (hereafter referred to as “boxes”) connected by plastic, electrically isolating tubing. TE elements are soldered directly to and sandwiched in between two boxes. No ceramic electrical isolation layer is needed since the current flows directly through the center of the device, from one side of a box through the copper fins and working fluid to the other side of a box. Each box becomes a separate thermally isolated region. Figure 1 shows such a heat exchanger assembly with seven TE elements and eight boxes. The boxes contain two sets of fins brazed inside, separated in the direction of flow from each other by 0.5 mm to create an offset fin effect. The

device is a liquid-liquid heat exchanger that can be connected in either counter or parallel flow.

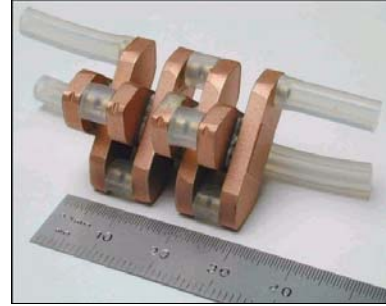


Figure 1: High-power density TE heat exchanger design.

Eliminating the ceramic electrical isolation layer provides almost direct contact with the working fluid for the particular configuration shown in Figure 1, which reduces the thermal losses of the system. By using thin TE elements and the boxes as connectors between the elements, the Joule heating component of the device is greatly reduced. The benefits of the high-power density heat exchanger design shown in Figure 1 are discussed in more depth by Bell [5].

Numerical Model

The numerical model of the TE heat exchanger uses a finite volume approach with discretization in the axial direction of both hot and cold flows. A first-order upwind differencing scheme is implemented for the convective derivatives. Transverse or radial heat transfer is modeled using standard conduction equations that incorporate central differencing discretization for the gradients. Each box is separated into five control volumes. Since the temperature gradients across each box and from one box to another are small, this level of discretization was determined to be adequate. Differential algebraic equations model the energy balances for each control volume. Figure 2 shows an example of a set of control volumes.

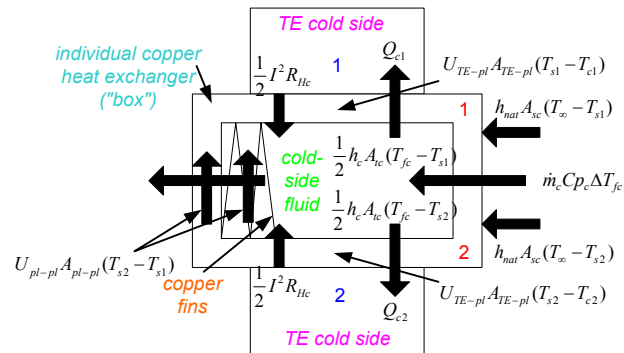


Figure 2: Schematic of energy flows in TE heat exchanger.

Energy balance equations for Figure 2 include the following:

$$Q_{c1} - U_{TE-pl} A_{TE-pl} (T_{s1} - T_{c1}) = 0 \quad (1)$$

$$U_{TE-pl} A_{TE-pl} (T_{s1} - T_{c1}) + h_{nat} A_{sc} (T_{s1} - T_{\infty}) - \frac{1}{2} I^2 R_{Hc} \quad (2)$$

$$-U_{pl-pl} A_{pl-pl} (T_{s2} - T_{s1}) - \frac{1}{2} h_c A_{tc} (T_{fc} - T_{s1}) = 0$$

$$\dot{m}_c C_p \Delta T_{fc} - \frac{1}{2} h_c A_{tc} (T_{fc} - T_{s1}) - \frac{1}{2} h_c A_{tc} (T_{fc} - T_{s2}) = 0 \quad (3)$$

$$\frac{1}{2} h_c A_{tc} (T_{fc} - T_{s2}) + \frac{1}{2} I^2 R_{Hc} - U_{TE-pl} A_{TE-pl} (T_{s2} - T_{c2}) \quad (4)$$

$$-h_{nat} A_{sc} (T_{s2} - T_{\infty}) + U_{pl-pl} A_{pl-pl} (T_{s2} - T_{s1}) = 0$$

$$U_{TE-pl} A_{TE-pl} (T_{s2} - T_{c2}) - Q_{c2} = 0 \quad (5)$$

where

$$Q_c = \alpha I T_c - K \Delta T_{TE} - \frac{1}{2} I^2 (R_{TE} + 2R_{int}) \quad (6)$$

Equations (1) and (5) are energy balance equations for conductive heat transfer from the TE elements into the boxes. Equations (2) and (4) are energy balance equations for conductive heat transfer from the box walls and fins to fluid convective heat transfer. They include the losses due to natural convection and Joule heating of the boxes. Equation (3) is an energy balance equation for the convective heat transfer into the fluid.

The model solves these governing equations simultaneously for the steady-state temperatures at each node in the directions of flow using the FSOLVE function in MATLAB, which incorporates an iterative Newton method. The number of simultaneous equations varies with the number of thermally isolated TE elements.

Due to the relatively low temperatures involved, radiation heat transfer and the Thompson heat component are neglected. Material properties are assumed to be temperature dependent. Convective heat transfer coefficient and pressure drop correlations were derived from experimental and simulation [6] data.

Model Validation

In order to demonstrate the range of performance of the TE heat exchanger and model, a wide variety of temperature and current conditions were tested. A sampling of these tests is shown in Figure 3. A heat exchanger assembly of fifteen TE elements and sixteen boxes was assembled and plumbed in a counterflow configuration. For each test point in Figure 3, both the hot and cold inlet temperatures were held constant at 30C. Inlet and outlet temperatures as well as end condition temperatures were measured with thermocouples and thermistors. Fluid (water for these tests) flow rates were measured by weighing a timed amount of fluid. The temperature differences on both the hot and cold sides of the device were chosen, and the flow rates were adjusted to obtain these differences at various currents.

The interfacial resistances, both electrical and thermal, for the TE devices were not known with significant accuracy. Thus, these two temperature independent parameters were determined so that the model's predictions best fit the experimental data. For the device tested whose results are

shown in Figure 3, the thermal and electrical interfacial resistances were determined to be $1e-7 \text{ m}^2\text{K/W}$ and $2.6e-10 \text{ } \Omega\text{-m}^2$ respectively. Both of these values are similar to those in the literature [7, 8].

Figure 3 shows that for a large range of currents, 100-600A, created by a variety of different temperature conditions, the TE heat exchanger can be simulated to within 7% accuracy for COP_c , where

$$COP_c = \frac{\dot{m}_c C_p \Delta T_{fc}}{Q_{in}} \quad (7)$$

$$Q_{in} = Q_h - Q_c = \alpha I \Delta T_{TE} + I^2 (R_{TE} + 2R_{int}) \quad (8)$$

To further confirm the model, values for hot and cold-side mass flow rates and TE input power were compared to experimental data. Error for cold-side mass flow was less than 5%. Hot-side mass flow error was less than 6%, and error for TE input power was less than 4%. Average error for each of these simulated values, including COP_c , was less than 3%.

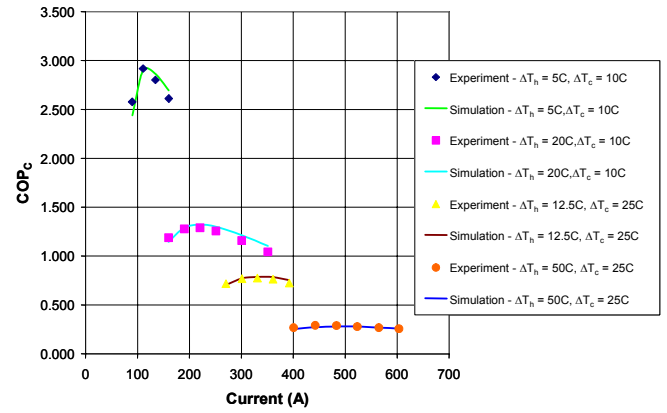


Figure 3: Graph showing the correlation between empirical and simulated data for COP_c .

In addition to the tests shown in Figure 3, over 50 additional tests were conducted on a variety of different heat exchanger assemblies, which included fifteen and seven element TE heat exchanger assemblies with either 2 mm or 6 mm tall boxes and with either 0.3 mm or 0.6 mm thick TE elements. Tests were also conducted on devices in a parallel flow configuration. Each of these additional tests matched the model's predictions with similar accuracy to those shown in Figure 3.

Pressure drop for the described heat exchanger was also modeled in order to use it as a constraint in optimization simulations. Figure 4 shows the results from these pressure drop tests. The trends of the graph indicate that the model captures the nature of the pressure drop behavior to within acceptable tolerances, especially at higher flow rates.

Graphical User Interface

In order to make the model more user-friendly, a graphical user interface (GUI) was created. The GUI is broken into four separate screens. On the MAIN screen, shown in Figure 5, the user can input fluid and TE properties along with temperature conditions. Flow direction, electrical polarity, and interfacial resistances can also be adjusted from the MAIN screen.

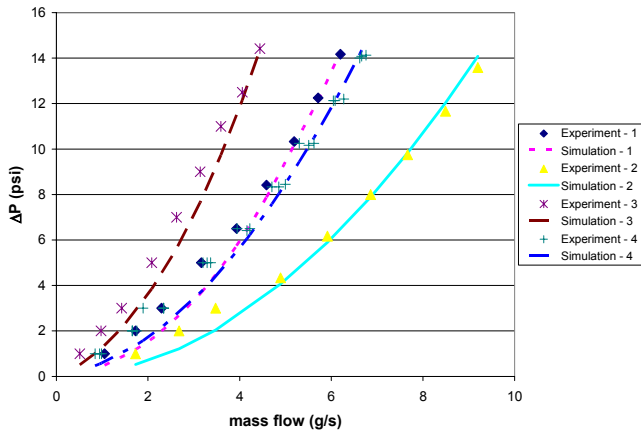


Figure 4: Graph showing the correlation between empirical and simulated data for pressure drop. 1) 8 boxes in series (6mm tall), 2) 4 boxes in series (6mm tall), 3) 16 boxes in series (2mm tall), 4) 8 boxes in series (2mm tall).

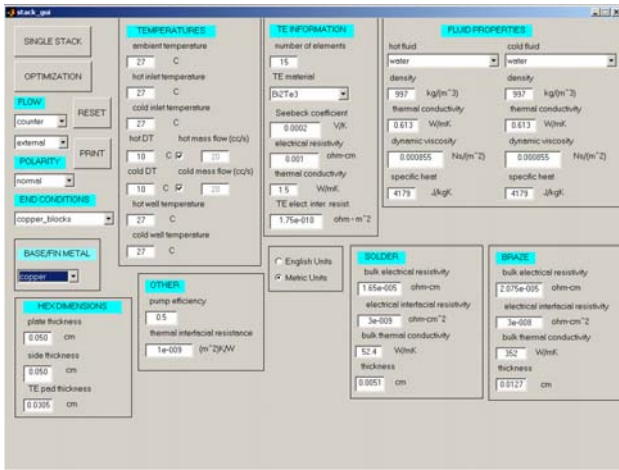


Figure 5: MAIN data input GUI.

To conduct an analysis of a set of temperature conditions for a single design configuration, the design engineer can proceed to the SINGLE ANALYSIS screen, Figure 6.

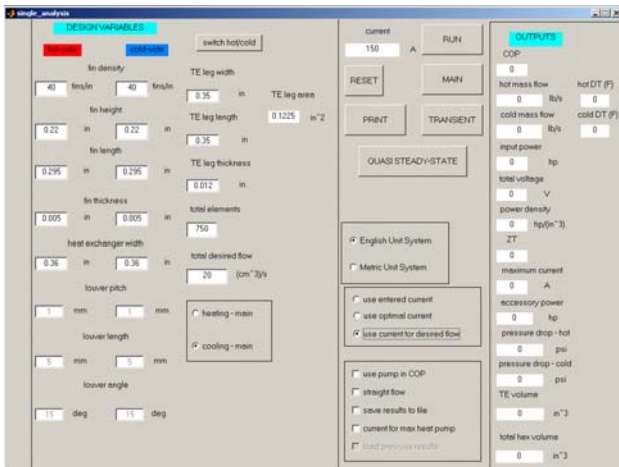


Figure 6: SINGLE ANALYSIS data input and output GUI.

On this screen, the dimensions of the hot and cold side boxes and TE elements can be adjusted. An analysis can be run to find the optimal current for a TE configuration or to find the current required to condition a desired flow rate given a desired number of total elements. The user can also enter a specific current or range of currents to analyze a design. Outputs displayed on this screen include COP, mass flow rates, TE input power, power density, TE figure of merit (ZT), fluid pressure drops, and TE and total heat exchanger volumes. If a range of currents is entered, three graphs, showing COP, TE input power, and mass flow rates, all vs. current, are displayed at the conclusion of the analysis.

Optimization

With the validated numerical model, critical design variables can be identified and varied to analyze the trade-offs necessary to improve COP. This process of perturbing design variables can be done through a trial-and-error parameter study or, more efficiently, by using advanced design optimization algorithms. Parametric studies can be useful, but they typically only look at one or two variables at a time. It becomes difficult to see the interaction between the different variables as they are changed in a design study. Advanced multi-parameter optimization allows for better understanding of the interactions between various design variables and parameters. The TE heat exchanger design problem, an example of a constrained, non-linear, minimization problem, is solved using the MATLAB function FMINCON, which uses a gradient-based optimization scheme.

The GUI shown in Figure 7 allows the user to input the starting point, upper and lower bounds, and additional constraints for an optimization study.

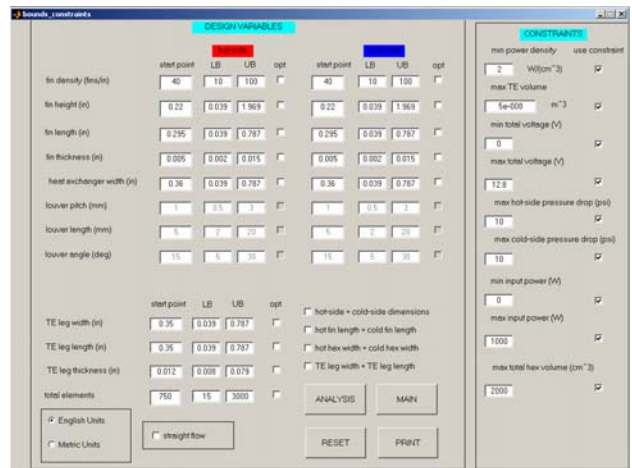


Figure 7: GUI for optimization analysis including data input for starting point, bounds, and constraints.

A design engineer can choose to optimize from fourteen different design variables, including fin and TE dimensions. A variety of different constraints can also be chosen, including maximum power density, TE and heat exchanger volume, hot- and cold-side pressure drops, and input power. Once the design variables and constraints have been chosen, an optimization analysis can be conducted with the same outputs as those shown in Figure 6.

Many different combinations of parameters and variables can be changed in order to optimize a design. The results of several optimal design combinations as well as the theoretical performance at a defined set of temperature conditions are shown in Figure 8. The results show that the design can realistically be optimized to achieve greater than 85% of the predicted theoretical performance.

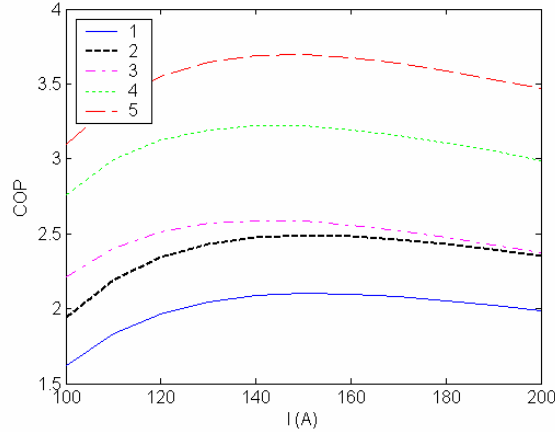


Figure 8: Example of optimization improvement. 1) base design, 2) same as 1 with optimal fin length and box width, 3) same as 2 with optimal fin height and TE area, 4) same as 3 with one tenth the electrical interfacial resistance, 5) theoretical performance using thermal isolation. Maximum pressure drop held constant for all cases.

Conclusions

The ability to model the TE system using thermal isolation to within 7% error for a wide range of conditions is one more step in reinforcing the benefits of thermal isolation in the direction of flow. Using the optimization analysis, the user can ascertain what design changes are needed to approach the theoretical performance defined in Bell [1].

By defining a model that has been sufficiently validated, a design engineer can use the optimization analysis to make quick optimal design changes and evaluate their performance effects without having to build repeated prototypes. The GUI allows the design engineer to use the model easily and quickly, improving design time and productivity. Thus, the model is a powerful tool for future TE heat exchanger designs. It enables the design engineer to maximize the advantages of the high-power density TE elements and the novel thermal isolation cycles.

Related work involves further development of this model, including the ability to simulate a number of different design configurations using similar design principles. These include additional liquid-liquid as well as air-air (already validated for one configuration), liquid-air, solid-liquid, and solid-air designs. A transient model of the TE system has also been created, and a model for TE power generation is currently under development.

Nomenclature

Parameters

- α Seebeck coefficient
- A_s, A_t heat transfer and total heat transfer surface areas
- C_p fluid specific heat

- h convective heat transfer coefficient
- I electrical current
- K TE conductance
- \dot{m} mass flow rate
- Q, Q_{in} heat flow and input power
- R_H, R_{TE}, R_{int} copper box, TE material, and interfacial electrical resistance respectively
- $T, \Delta T$ temperature and temperature difference
- $U_{TE-pl}, A_{TE-pl}; U_{pl-pl}, A_{pl-pl}$ overall conduction heat transfer coefficient and heat transfer area between respectively the TE and plate surfaces and between the two box plate surfaces, including the box walls and fins

Subscripts

- $I-2$ reference to particular TE or surface from Figure 2
- ∞ ambient
- f fluid
- h, c hot or cold-side
- nat natural convection

Acknowledgments

The author would like to thank several individuals: Dr. L. Bell for his inspiration, overall guidance, and review of equations and text; Mr. R. Diller and Mr. A. Nannini for reviewing the text, model discussions, and model testing; Mr. R. Giroux for model testing; Mr. J. Lofy for additional model discussions; Dr. R. Golbert for proofreading the text; and Ms. M. Banda for document preparation.

References

1. Bell, L. E., "Use of Thermal Isolation to Improve Thermoelectric System Operating Efficiency," *21st International Conference on Thermoelectrics*, Long Beach, CA, Aug. 25-29, 2002, pp. 477-487.
2. Diller, R. W. and Chang, Y. W., "Experimental Results Confirming Improved Performance of Systems Using Thermal Isolation," *21st International Conference on Thermoelectrics*, Long Beach, CA, Aug. 25-29, 2002, pp. 548-550.
3. Crane, D. T., Optimizing Thermoelectric Waste Heat Recovery from an Automotive Cooling System, University of Maryland, College Park, (2003)
4. Crane, D. T. and Jackson, G. S., "Optimization of Cross Flow Heat Exchangers for Thermoelectric Waste Heat Recovery," *Energy Conversion and Management*, Vol. 45, No. 9-10 (June 2004), pp. 1565-1582.
5. Bell, L. E., "High Power Density Thermoelectric Systems," *23rd International Conference on Thermoelectrics*, Adelaide, AU, July 25-29, 2004, pp. TBD.
6. Faulkner, F., COLDPLT.exe, Thermodynamics Analysis Service (Hobe Sound, FL, 1999)
7. Min, G. *et al*, "Determining the Electrical and Thermal Contact Resistance of a Thermoelectric Module," *11th International Conference on Thermoelectrics*, Arlington, TX, October 7-9, 1992, pp. 210-212.
8. Nolas, G. S. *et al*, Thermoelectrics - Basic Principles and New Materials Developments, Springer (Verlag Berlin Heidelberg, 2001), pp. 170,253.